Ultrasound in Med. & Biol., Vol. 34, No. 9, pp. 1396–1407, 2008

0301-5629/08/$–see front matter

ELSEVIER

doi:10.1016/j.ultrasmedbio.2008.01.017

● *Original Contribution*

HIGH FREQUENCY ULTRASOUND TISSUE CHARACTERIZATION AND ACOUSTIC MICROSCOPY OF INTRACELLULAR CHANGES

SEBASTIAN BRAND,*†‡ EIKE C. WEISS,§ ROBERT M. LEMOR,§ and MICHAEL C. KOLIOS*†¶

*Physics Department, Ryerson University, Toronto, Canada; †Ontario Cancer Institute, Princess Margaret Hospital, Toronto, Canada; ‡Q-BAM Laboratory, Halle/S., Germany; §Fraunhofer Institut fuer Biomedizinische Technik, St. Ingbert, Germany; and ¶Department of Medical Biophysics, University of Toronto, Toronto, Canada

(*Received* 11 *September* 2007; *revised* 27 *December* 2007; *in final form* 29 *January* 2008)

Abstract—The objective of this work is to investigate changes in the acoustic properties of cells when exposed to chemotherapy for monitoring treatment response. High frequency ultrasound spectroscopy (10-60 MHz) and scanning acoustic microscopy (0.9 GHz) were performed on HeLa cells (Ackermann et al. 1954, Masters 2002) that were exposed to the chemotherapeutic agent cisplatin. Ultrasonic radio-frequency data were acquired from pellets containing HeLa cells after exposure to cisplatin to induce apoptosis. Scanning acoustic and laser fluorescence microscopy images were recorded from single HeLa cells exposed to the same drug. Data acquisition in both cases was performed at several time points throughout the chemotherapeutic treatment for up to 27 h. In the high frequency ultrasound investigation, normalized power spectra were calculated within a region-of-interest. A 20 MHz transducer (f-number 2.35) and a 40 MHz transducer (f-number 3) were used for the data collection in the high frequency ultrasound experiments. The backscatter coefficients, integrated backscatter coefficients, mid-band fit and spectral slope were computed as a function of treatment time to monitor acoustical property changes during apoptosis. Acoustic attenuation was measured using the spectral substitution technique at all time points. Spectral parameter changes were detected after 12 h of exposure and coincided with the initiation of cell damage as assessed by optical microscopy. Integrated backscatter coefficients increased by over 100% between 0 h and 24 h of treatment, with small changes in the associated attenuation (~0.1 dB/[MHz cm]). Acoustic microscopy was performed at 0.9 GHz frequency. The cell structure was imaged using staining in laser fluorescence microscopy. All cells showed excellent correspondence between the locations of apoptotic nuclear condensation observed in optical imaging and changes in attenuation contrast in acoustic microscopy images. The time after drug exposure at which such changes occurred in the optical images were coincident with the time of changes detected in the acoustic microscopy images and the high frequency ultrasound experiments. (E-mail: Sebastian.Brand@gmail.com) **© 2008 World Federation for Ultrasound in Medicine & Biology.**

Key Words: **High frequency ultrasound, Acoustic microscopy, Viable cells, Quantitative ultrasound.**

INTRODUCTION

Within the last 50 years ultrasonic imaging has seen an increase in utilization for diagnostic and therapeutic purposes. Sound waves in the frequency range from 100 kHz to 15 MHz have been used in medical diagnostics as well as therapy. The most popular way of displaying backscatter information is B-mode imaging. This technique uses the envelope of detected ultrasound echoes from a region-of-interest (ROI) to create gray- scale images which display a cross-sectional mapping of the echo intensity. However, these images only use a fraction of the information contained in the signal, as the backscatter frequency and phase information is not used in conventional B-mode imaging.

Several investigators have suggested that the frequency dependent information in ultrasound echo signals can be related to acoustical and structural properties of tissue microstructure (Feleppa et al. 1986; Insana et al. 1990; Lizzi et al. 1988, 1997a; Nicholas 1982). Spectral analysis of radio-frequency (RF) ultrasound signals can provide information about the tissue properties like the frequency dependent attenuation (Kuc 1985; Madsen et al. 1999) the frequency dependence of the backscatter (Waters et al. 2003) and (using these two parameters) the effective scatterer size (Lizzi et al. 1986). In general, the

Video Clips cited in this article can be found online at: http://www.umbjournal.org.

Address correspondence to: Dr. Sebastian Brand, Martin-Luther University of Halle, Dept. of Orthopaedics, Q-BAM Laboratory, Magdeburger St. 22 06112 Halle/S Germany. E-mail: Sebastian.Brand@gmail.com

frequency dependent attenuation is related to the bulk composition of the tissues, while the frequency dependence of the backscatter is related to the structure of the biological scatterers. Tissue characterization using ultrasound has been performed for *in vivo* prostate, testis (Feleppa et al. 1996, 1999, 2000; Jenderka et al. 1999, Lizzi et al. 1997b), liver (Lang et al. 1994; Lu et al. 1999; Lizzi et al. 1997b; Oosterveld et al. 1991), ophthalmologic tissue (Feleppa et al. 1986; Thijssen 1993; Verbeek et al. 1994) and the myocardium (Dent et al. 2000; Zuber et al. 1999). Apart from characterizing tissue pathologies for diagnosis, ultrasonic tissue characterization has also been used for classifying the quality of meat, defined by the content of intramuscular fat (Brand et al. 2002, Moerlein et al. 2005). Most of these studies used ultrasonic backscatter signals to extract tissue acoustic properties and related them to specific pathologic alterations of the investigated specimen. Especially the group of Lizzi et al. (Lizzi et al. 1983, 1986, 1997a, 1997b) pioneered detailed theoretical formulations for extracting tissue acoustic information and the link to the underlying microstructure from backscattered ultrasonic signals.

A small number of previous investigations have examined the frequency dependence of ultrasound backscatter combined with its relation to the underlying tissue structure *in vivo* in the frequency range above 15 MHz. However, recent developments in transducer technology and electronics enabled the availability and application of ultrasound in the frequency range above 20 MHz (Cloutier et al. 1997; Foster et al. 2000; Silverman et al. 1995, 2001; Ursea et al. 1998). As the ultrasound wavelength approaches the size of the cells, it is expected that ultrasound based techniques are more sensitive to structural changes at a cellular level. Indeed, experimental data and effective scatterer size estimates derived from the frequency dependence of ultrasonic backscatter signals, using models developed by Lizzi and coworkers, indicate that the size of the dominant scatter source is on the order of a cell or its' nucleus (Lizzi et al. 1983, Kolios et al. 2002, 2003).

The interaction of ultrasound with biological tissue is determined by the mechanical properties of the underlying structure. In soft tissues, this structure is composed primarily of a cellular matrix containing single cells in an aggregate. Ultrasonic scattering is caused by structures below and up to the order of the ultrasound wavelength. Scattering effects that can be observed in the frequency range from 10 to 100 MHz may have their origin in structures at a subcellular level (Briggs 1995). Thus, investigating the mechanical properties on a single cell base will potentially provide insight in the mechanism of scattering from cellular ensembles, such as tumors (Kolios et al. 2002, Czarnota et al. 1997). Scanning acoustic microscopy (SAM) enables the investigation of viable cells *in vitro* on a microscopic scale offering the potential to explore mechanical properties. Using frequencies up to 2 GHz resolutions of 1 μm can be achieved (Briggs 1992). A detailed description of these methods can be found elsewhere (Briggs 1992, 1995, Kundu et al. 2000, Kundu 2004). Ultrasonic properties that can be measured in these experiments include sound velocity, sound attenuation, cell thickness but also the elasticity and stiffness of intracellular components (Bereiter-Hahn et al. 1995, 1998; Zoller et al. 1997).

Two different approaches are used in SAM: time resolved SAM (Briggs et al. 1993, Lemor et al. 2003, Weiss et al. 2007) and V(z) (Bereiter-Hahn et al. 1998, Kundu et al. 1992) or V(f) (Kundu et al. 2000) techniques. Time resolved acoustic microscopy applies a short broad band pulse and seems the most promising approach for quantitative measurements. However, the analysis requires the separation of acoustic pulses which potentially overlap (Briggs 1995). Another method known as reflection confocal acoustic microscopy (applying a monochromatic tone burst) enables the acquisition of V(z) or V(f) signatures. A comprehensive theoretical background and contrast theory is readily available (Briggs 1992). However, these techniques require data collection at multiple defocus positions. This creates problems when the transducer approaches the cell as it causes shear stress due to the scanning motion. Moreover, the acquisition of data at multiple depths significantly increases the data acquisition time. As opposed to light microscopy, in SAM, the contrast arises from the mechanical properties of the cellular substructure and potentially other physical effects (surface wave modes on the substrate, interference fringes due to modulation of the substrate echo by the cell surface echo and so on). The rich contrast produced by acoustic property variations negates the need for the use of specialized and potentially toxic dyes that are used in light microscopy.

Major changes in cell morphology occur after chemotherapeutic treatment. Apoptosis is a type of cell death that is induced by the cell itself. The cell undergoes significant morphological changes, such as nuclear condensation and fragmentation as well as membrane blebbing and overall cell shrinkage. A range of techniques have been developed to identify cells undergoing apoptosis using biochemical assays. These techniques are widely used to assess and identify apoptosis in cultured cells and in fixed tissues. However, there are very few reliable techniques for the noninvasive assessment of apoptosis in live un-sectioned tissues. Yet, this is critical for assessing the response of tumors to anticancer therapies, like chemo- or radiation treatment. Since multiple ultrasonic imaging sessions do not carry the increased risks that other modalities used for apoptosis monitoring do, such as positron emission tomography (PET) (Lahorte et al. 2004), scanning procedures can be performed

rapidly for monitoring the treatment response over an extended period of time.

It was shown previously that intracellular changes resulting from exposure to the chemotherapeutic agent cisplatin can be detected using high frequency ultrasound (Czarnota et al. 1997, 1999; Kolios et al. 2002). These studies used acute myeloid leukemia (AML) cells. Whereas individual cells cannot be resolved in the frequency range between 10 MHz and 60 MHz, an increase in the backscatter intensity and changes in the spectral parameters of AML cell ensembles were observed. It is not clear however whether the morphological changes clearly observed in optical microscopy at the single cell level correspond to changes in the cell acoustical properties. It is tempting to relate the large changes in apoptotic nuclear structure to the ultrasound backscatter changes, as our experiments to date suggest the nucleus as the main scattering source of cell ensembles (Taggart et al. 2007, Kolios et al. 2002, 2003). However, we have also shown theoretically that changes in the spatial organization of the scatterers can also induce the observed changes in ultrasound backscatter (Hunt 2002) and potentially changes in spectral slopes (Hunt, personal communication, 2004). The AML cell line used in previous studies is not an epithelial cell line that forms solid tumors but a hematologic malignancy. However, the ultrasonic techniques our group is developing are intended to image solid tumors. Moreover, as the AML cell line is not adherent, it cannot be used in acoustic microscopy studies.

To investigate changes in ultrasound backscatter of an epithelial cell line and, also, further probe changes in acoustical parameters at a single cell level applying acoustic microscopy, a cervix carcinoma cell line (HeLa) was used (Ackerman et al. 1954; Masters et al. 2002). Cell death was induced by exposure to a chemotherapeutic drug and cell pellets were scanned at several time points after treatment using high frequency ultrasound (20 and 40 MHz transducers). Spectral parameter estimation methods were applied to the radio-frequency (RF) ultrasound signals, acquired from pellets of HeLa cells. For further investigation on a cellular level, a novel device that combined optical and acoustical microscopy was used. Laser fluorescence and scanning acoustic microscopy imaging was performed on treated HeLa cells. The acoustic microscopy applied ultrasound at 0.9 GHz center frequency with a pixel spacing of 0.16 μm, thereby allowing us not only to detect changes in intracellular acoustical parameters but also to compare these changes with the corresponding variations observed in the optical images of the same cell.

METHODS

Cell culture preparation

In the experiments using both high frequency ultrasound and acoustic microscopy HeLa cells obtained from ATCC (American Type Culture Collection, Manassas, VA, USA) were used. This is a rapidly growing human cervix carcinoma cell line and has been previously explored to investigate changes during cell death (Maldonado et al. 1995). The chemotherapeutic agent cisplatin was used for inducing apoptosis in HeLa cells. HeLa cells exposed to cisplatin undergo cell death, presenting morphological and biochemical characteristics typical of apoptosis (Velazquez et al. 1998, Maldonado et al. 1995). Cells were thawed from frozen stock and cultured in cell culture flasks containing 15 ml of minimum essential media (MEM) supplemented with 10% of heat inactivated fetal bovine serum (FBS) and 0.1% gentamycin (antibiotic) in a humidified atmosphere containing 5% CO_2. Cell death was induced in HeLa cells by adding 150 μg cisplatin into the medium of each flask to provide a final concentration of 10 μg/ml.

In the high frequency ultrasound experiments, HeLa cells were exposed to cisplatin for 0, 8, 12, 18 and 24 h before data acquisition and imaging. Cells were trypsinized, centrifuged at 216 *g* and the medium was removed. Following this, the cells were then resuspended in phosphate buffered saline (PBS) and centrifuged in a custom made two-chamber holder (Fig. 1) to a final pellet at 1942 *g*. The pellet had a diameter of 3 mm and a height of approximately 1 mm. At the bottom of the two-chamber holder, a polished quartz substrate was used for calibration purposes. During ultrasonic investigations cell pellets were submerged in PBS.

In preparation for acoustic and optical microscopy, HeLa cells were cultured in cell culture coverslip-dishes, containing 5 ml of the described medium. Apoptosis was induced by exposing the cells to a concentration of 10 μg/ml cisplatin. During experiments, the adherent cells were submerged in the medium. For laser fluorescence microscopy two different dyes, Hoechst 33342 and DIOC 3(5) were added to the medium. Hoechst 33342 binds to chromatin providing structural information about the cell nucleus and DIOC 3(5) attaches to inner cellular membranes providing structural information about the cytoplasm.

High frequency ultrasound experiments

Experimental set-up. Ultrasonic imaging and RF data acquisition were performed with an ultrasound biomicroscope (UBM) (VS40B, VisualSonics Inc., Toronto, Canada), using two different transducers, to cover an expanded frequency range. Transducer specifications are given in Table 1. The use of two transducers not only provided an extended frequency range (from 10 MHz to 60 MHz) but allowed the verification of the independence of the normalized RF data from the system transfer characteristics.

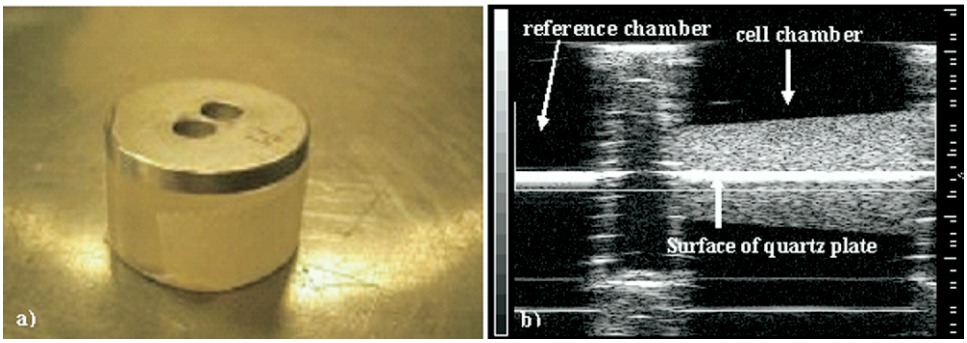

Fig. 1. (a) Two chamber holder used in the high frequency ultrasound experiments. The bottom is a flat quartz cylinder. Cell pellets are placed in one chamber of the metal holder, while only the coupling medium is in the second chamber. (b) An ultrasound image of the two-chamber holder. The left chamber contains PBS, and the right chamber contains a HeLa cell pellet. The major division on the right hand side scale bar in the ultrasound image is 1mm. The arrowhead to the far right of the image indicates the transducer focus.

The UBM enabled real-time B-mode imaging of the prepared biological specimen. Unprocessed RF ultrasound signals were sampled at 500 MHz by the A/D converter unit of the UBM (input range: ±250 mV, sample resolution: 8 bit). Cell pellets were imaged at five time points after exposure to the chemotherapeutic drug (0 h, 8 h, 12 h, 18 h and 24 h) and a total of 255 RF lines were recorded at three scan planes that were separated by at least one beam width. The length of each scan line was approximately 3-4 mm. One chamber of the custom-made two chamber holder contained the cell pellet while the second camber was left empty for assessing the reference signals. The two-chamber holder (shown in Fig. 1) was submerged in PBS that acted as the coupling medium for the ultrasonic wave propagation. Since the two chambers were adjacent to each other, RF signals were acquired in the same scan from the cell pellet and the PBS containing chamber (reference chamber).

For analyzing the reflections from the surface of the quartz substrate (part 43424, Edmund Industrial Optics Inc., Barrington, NJ, USA) a transducer appropriate electronic attenuator (HAT20+, HAT15+, Mini-Circuits, New York, NY, USA) was placed in the receive path of the UBM, to match the signal intensity obtained from the quartz surface to the input range (±250 mV) of the UBM's internal A/D-converter unit. In addition to the three scans recorded from the cell pellet (without the attenuator), three scan planes from both chambers were acquired for estimating the attenuation of the cell pellet (with the attenuator) from the reflection of the quartz substrate behind the cell pellet relative to the signal recorded at the reference chamber. When recording the RF-data for the attenuation measurements, the transducer specific focus was placed on the surface of the quartz substrate. This experimental sequence provided for each transducer and each time point, three sets of RF data for analyzing the scattering from within the cell pellets as well as three sets of RF signals for analyzing the quartz plate reflections and attenuation estimation. All experiments were performed at room temperature (21 ±1°C) and adjacent scan planes were separated by at least one beam width in order to obtain statistically independent RF-signals.

Table 1. Specifications of the ultrasound transducers used for the high frequency ultrasound experiments

Transducer description	20 MHz	40 MHz
Center frequency (f_c)	19.25 MHz	37.5 MHz
Bandwidth (BW)	100%	98%
f-number	2.35	3
Diameter of transducer aperture	8.5 mm	3 mm
Depth of focus	3.2 mm	2.5 mm

Data analysis

Signal analysis and parameter calculation was performed off-line using a custom-made MATLAB (Mathworks, Natick, MA, USA) program. This program enabled the visualization of the RF data similar to a B-mode image and was used to select a region-of-interest. For the estimation of scattering characteristics, the ROI enclosed only signals from within the cell pellet. This ROI contained approximately a total of 100 RF lines from three different scan planes and had a physical length of 1 mm. For estimating averaged parameters, one ROI was chosen within each ultrasound scan that were recorded without the attenuator in the receive path of the UBM. This results in a total of three ROIs for each time point during the treatment. The RF lines were analyzed using a sliding window algorithm provided by the custom-made MATLAB software. The window length was transducer specific and set to be eight times the wavelength of the center frequency of the transmitted pulse

for the 20 MHz transducer and 16 times the wavelength for the 40 MHz transducer. The step width between two sequential window positions was 30 μm. A rectangular window function was used and the effect of the gate-edge on the spectral data was compensated for by using the algorithm proposed by Oelze et al. 2004. The Fourier transform was applied to each windowed signal within the ROI and the power spectra were obtained by averaging the results of all window positions and all RF lines. Prior to averaging, each calculated spectrum was compensated for attenuation and the transducer specific diffraction pattern. The axial amplitude distribution was obtained from an untreated pellet of HeLa cells. After estimating the frequency dependent attenuation as described below, the axial diffraction pattern was computed (Gärtner et al. 1996). For deriving a compensation function all power spectra of the reference cell pellet were computed, attenuation compensated and normalized to the maximum spectrum, which occurs at the focus. This compensation function estimates the diffraction pattern in a homogenous medium under the same conditions as the cell experiments were performed. Normalizing this to the attenuation compensated power spectrum at the focus preserves the spectral shape of the measured spectra to which the compensation function is applied. Assuming that the attenuation corrected spectrum at the focus is only dependent on the systems impulse response and the scattering characteristics, the normalized compensation function only contains the depth specific spectral shape variations caused by the diffraction pattern.

Compensation of the diffraction pattern was performed using a depth equivalent spectrum from the compensation function FC (f, z), where f represents the frequency and z the axial distance from the transducer surface. The power spectra were then normalized to the power spectrum of the quartz reflector (Lizzi et al. 1983). This reference was obtained from a flat quartz cylinder placed at the focus for each individual transducer (reference chamber).

Spectral parameters were obtained from the averaged power spectra after normalizing to the transducer specific reference. Linear regression analysis was then applied to the normalized power spectra. The slope and the mid-band fit of this analysis were measured (Lizzi et al. 1983). To compare the data with more standardized backscatter parameters, the backscatter coefficients and the integrated backscatter coefficients were also computed (Turnbull et al. 1989, Worthington et al. 2001). For estimation of backscatter coefficients the attenuation inside the ROI was taken into account. Attenuation in the path of sound propagation, between the transducer and the cell pellet was compensated for, by using an attenuation value obtained by a reference pulse that was recorded from a quartz plate at the focus using the same coupling medium (PBS).

Acoustic attenuation was estimated using the spectral substitution technique (Kuc et al. 1985). This method analyzes the spectral signal intensity reflected from a reference material that is placed at the transducers' focus, behind the attenuating medium. This signal then is compared with a reflection from the same reflector at the same distance to the transducer after traveling through a medium with known attenuation. In this study, we used the reflection from a flat quartz cylinder that was the bottom of the two-chamber holder (Fig. 1). The power spectra from the quartz reflection of the chamber that contained the cell pellet and the reflection of the quartz surface measured from the chamber containing the PBS were computed and subtracted. The quartz surface was placed at the focal plane of each transducer. Signals of the receive path were attenuated by 35 dB (HAT20+ and HAT 15+) for the 20 MHz transducer and by 20 dB (HAT20+) for the 40 MHz transducer to adapt the signal amplitude to the input range of the A/D converter of the UBM. Power spectra in each chamber were estimated by averaging 80 RF lines that contained the pulse from the quartz surface. Following this, spectra in the log-domain were subtracted and attenuation was estimated as a function of frequency. By normalizing the obtained attenuation spectra to the thicknesses of the individual cell pellets, attenuation spectra in dB/cm were derived. Linear regression analysis provided the attenuation coefficients in dB/(MHz cm). The thickness of the cell pellets was estimated from the reconstructed B-mode images using a speed of sound value of 1540 m/s (Duck 1990).

Acoustic microscopy

A novel acoustic microscope (SASAM, Fraunhofer Institute for Biomedical Engineering, St. Ingbert, Germany) was used for microscopic investigations at the single cell level. The SASAM combines a scanning acoustic microscope, a phase contrast microscope and a laser fluorescence microscope in one device (Lemor et al. 2003, 2004). The optical unit is based on an Olympus IX 81 microscope (Olympus, Tokyo, Japan).

After adding the fluorescence markers to the medium, scanning acoustic microscopy and optical imaging were performed. Hoechst-33342 was used for visualization of condensed chromatin in laser fluorescence. Intracellular membranes were labeled using the fluorescence marker DIOC5(3). In addition, phase contrast imaging of the investigated cells was performed. A CCD camera with 672 x 512 elements was used to capture the images that had a resolution of 0.32 μm.

Scanning acoustic microscopy was performed with a highly focused ultrasonic transducer (0.8-1.3 GHz, KSI, Herborn, Germany) at 0.9 GHz center frequency. The transducer lateral resolution was approximately 1.5 μm in water. During the scanning process, the transducer

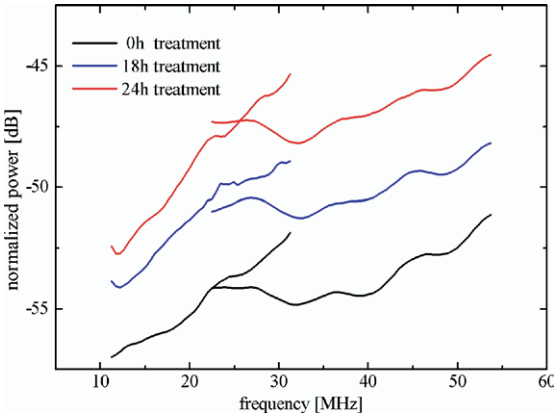

Fig. 2. Normalized backscatter power spectra of HeLa cells derived using the backscatter from two different transducers (20 MHz and 40 MHz), before treatment and after 18 h and 24 h of exposure to cisplatin.

unit was moved in a plane parallel to the coverslip on which the cells were adhered. For each acoustic scan 350 x 350 measurements were performed to create the image. The spacing between the transducer positions was 0.16 μm and the dimensions of the resulting images were 56 μm x 56 μm. At each position, an ultrasonic pulse (center frequency 0.9 GHz, relative bandwidth of the pulse 250 MHz) was emitted and the received echoes were digitized using an A/D-converter (DC211, Acqiris, Geneva, Switzerland). The sampling frequency was 4 GHz and the ADC's bandwidth was 1.1 GHz. Received signals were windowed at the position of the glass plate, using a rectangular window, in order to estimate the reflection of the coverslip. The resulting acoustic image shows the intensity of the reflected pulse and, thus, is representative of acoustic attenuation through the sample, which includes sample absorption and scattering. Scans were repeated five times in order to estimate averaged intensity values. The total time for recording the acoustical image was approximately 5 min.

In a second experiment, the acoustic microscope was run in automatic mode and repeatedly scanned three separate regions inside the cover-glass dish. During the experiments, cells were exposed to cisplatin and scans were performed every 15 min for a total duration of 27 h allowing the creation of an animation (Supplementary video 1). Throughout all microscopic experiments cells were kept at 37 $\pm$ 0.2°C in a humidified atmosphere containing 5% CO_2.

RESULTS

High frequency ultrasound experiments

In Fig. 2, the normalized power spectra of backscattered ultrasound from HeLa cells undergoing cell death are shown for three experiment time points (pretreatment, 18 h, 24 h). Plotted are the results obtained from measurements with the 20 MHz and 40 MHz transducer. It can be seen from Fig. 2 that normalized power spectra overlap and show acceptable trend continuity for the two transducers at each time point, despite the different transducer geometries and attention path length through the coupling medium (Table 1). The normalized power spectra show an increase in backscatter as a function of treatment time for both transducers.

In Fig. 3a, the spectral slopes of the normalized power spectra are plotted as a function of cisplatin exposure, calculated from the linear regression analysis of the normalized power spectra. For data acquired with the

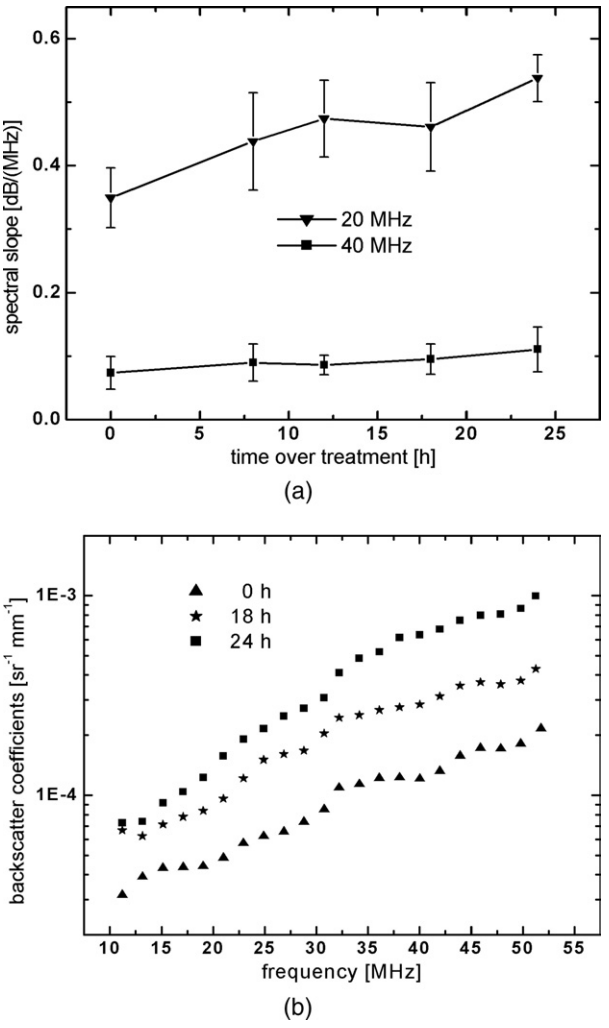

Fig. 3. (a) Spectral slope of the normalized power spectra from HeLa cell backscatter as a function of treatment time, estimated from two different transducers (20 MHz and 40 MHz). (b) Backscatter coefficients at three different time points as a function of frequency in the range from 10 MHz to 52 MHz. The error bars in (a) represent the standard deviations between the scans.

20 MHz transducer, spectral slopes increased monotonically from 0.35 ± 0.03 dB/MHz pretreatment to 0.52 ± 0.04 dB/MHz at the 24-h time point of the chemotherapy. To test for treatment-time related changes of the spectral slope values, analysis of variance (ANOVA) was applied to the slope estimates. From the 20 MHz experiments, a significant increase ($p < 0.05$) of spectral slope values from 0.35 dB/MHz to 0.52 dB/(MHz) was observed. For the 40 MHz experiment, an insignificant ($p = 0.167$) increase from 0.07 dB/MHz at 0 h to 0.11 dB/MHz at 24 h was measured.

Figure 3b plots the backscatter coefficients as a function of frequency for the pretreatment, the 18-h and the 24-h time point. Backscatter coefficients increase as a function of frequency and treatment time. Parameters describing the energy of the backscattered ultrasound are represented as a function of time in Fig. 4a. The integrated backscatter coefficient (IBC) values show a significant increase of more than 100% as a function of treatment time. The corresponding changes in mid-band fit are displayed in Fig. 4b), in which values increase significantly ($p < 0.05$) by 5.3 dB for the 20 MHz data and by 7 dB for the 40 MHz data between untreated cells and cells exposed to cisplatin for 24 h.

Figure 5 shows acoustic attenuation of HeLa cell pellets, estimated from the reflections of the quartz-cylinder at the bottom of the two-chamber holder. In Fig. 5a, attenuation is plotted as a function of frequency for the 20 MHz and 40 MHz transducers at the time points 0-h, 18-h and 24-h post-treatment. Attenuation increased as a function of treatment time for both transducers used. In Fig. 5b, the slope of the acoustic attenuation (from Fig. 5a) is plotted in dB/(MHz cm) as a function of treatment time for the 20 MHz and 40 MHz transducers. The values of the slope of the attenuation of the 40 MHz transducer slightly increase throughout the experiment from approximately 0.6 ± 0.06 dB/(MHz cm) to 0.7 ± 0.08 dB/(MHz cm). Attenuation values for the 20 MHz transducer are lower and increase from 0.22 ± 0.05 dB/(MHz cm) to 0.36 ± 0.07 dB/(MHz cm). ANOVA was applied to the estimation results and p values below 0.05 were obtained.

Acoustic microscopy

In Fig. 6, images of acoustic microscopy of HeLa cells at different time points during the cisplatin exposure are shown. Acoustic contrast increases as a function of time. The cell interior becomes darker (more attenuating) and less regular in shape as time increases. At the 18-h and 25-h time points, an increasing number of cells show nonregular-shaped and highly attenuating structures in the cell interior (Supplementary video 1).

Laser fluorescence microscopy and simultaneous acoustic microscopy of HeLa cells was performed in a separate experiment. In Fig. 7, images of acoustic and laser fluorescence microscopy are shown. From the left to the right, imaging was performed at 0 h, 12 h and 25 h after initiating the treatment. The bottom row shows the fluorescence microscopy images where membranes are stained green (dye: DIOC 5(3)) and nuclei are stained blue (dye: H33342). The H33342 dye attaches to condensed chromatin and appears brighter when nuclei condense. The rectangle in the fluorescence microscopy images represents the region where the acoustic microscopy was performed. The physical dimension of that region is 56 μm x 56 μm.

In the acoustic microscopy images, cells responding to the treatment decreased in diameter, forming irregular

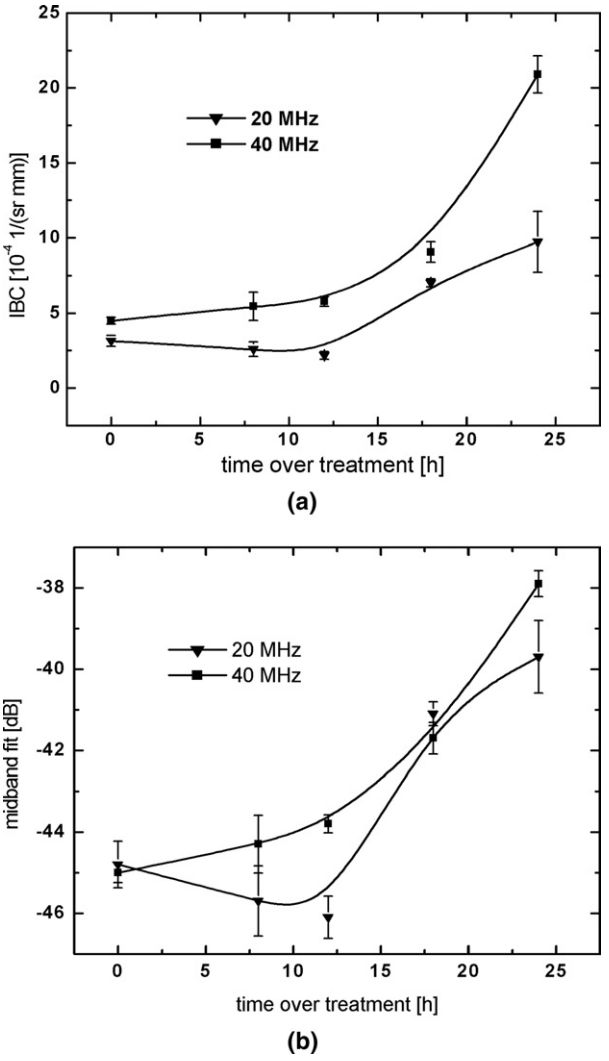

Fig. 4. Backscatter intensity of normalized power spectra as a function of treatment time, estimated in two different frequency ranges. (a) Integrated backscatter coefficients. (b) Mid-band fit of normalized power spectra. Error bars represent the standard deviation between the scans.

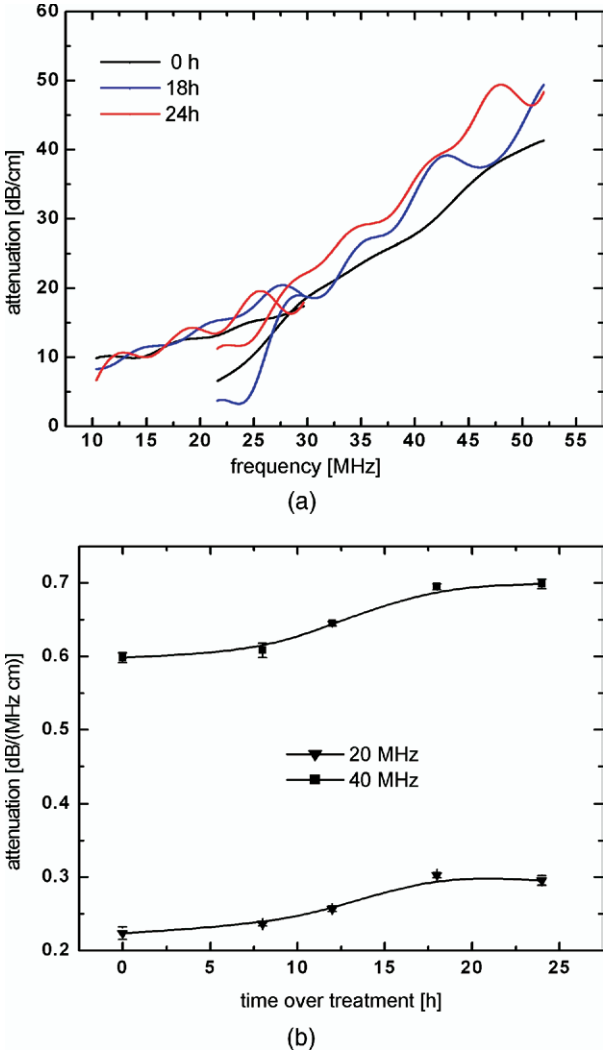

Fig. 5. Acoustic attenuation of HeLa cells as a function of cisplatin exposure time. (a) Attenuation spectra for two different transducers (20 MHz and 40 MHz) plotted as a function of frequency at three time points (0 h, 18 h and 24 h). (b) Attenuation coefficients in (dB/[MHz cm]) as a function of treatment time estimated in two different frequency ranges. Error bars represent the standard deviation between the scans.

shapes and appear darker than nonresponding cells. From the laser fluorescence images, it can be observed that all cells, which appear darker in the acoustic images, show fluorescent staining patterns indicative of apoptosis. In all samples collected (not all images shown), there is an excellent correlation between cells undergoing apoptosis as assessed by fluorescence staining and the cells that display an increased acoustic attenuation measured by acoustic microscopy. Since the brightness in the acoustic images is directly related to the ultrasonic intensity reflected from the glass substrate, darker regions indicate a lower intensity of the reflected pulse. The middle column in Fig. 7 shows responding and nonresponding cells in the same image and, thus, allows a direct comparison of acoustic properties of cells undergoing apoptosis and cells not responding to the treatment.

DISCUSSION AND CONCLUSION

High frequency ultrasound experiments

In ultrasound spectroscopy, increases in the backscattered intensity from HeLa cells were observed after exposure to cisplatin. Similar results were obtained from ultrasonic imaging of acute myeloid leukemia (AML) (Czarnota et al. 1997; Kolios et al. 2002) and epithelial cells (HEp-2) (Brand et al. 2006) during treatment. These frequency dependent increases were 10 dB for AML (Kolios et al. 2002) and 7 dB for HEp-2 (Brand et al. 2006) cells. Similar increases in backscatter were measured for the HeLa cells. The data analysis allowed a direct comparison between various parameters used in the field of ultrasonic tissue characterization. Integrated backscatter coefficients (a measure of backscatter intensity) display a trend similar to that of the mid-band fit as a function of treatment time for all examined frequency ranges. Integrated backscatter from the 20 MHz data increased from 3.27 10^{-4} sr^{-1} mm^{-1} pretreatment to a maximum of 9.77 10^{-4} sr^{-1} mm^{-1} after 24 h of treatment, whereas values of the mid-band fit showed a maximum of −40 dB at the 24-h time point, 4.5 dB higher than at the pretreatment time point (Fig. 4) and consistent with changes observed with other cell lines. Therefore, the backscatter increase as a function of cisplatin treatment also holds for this epithelial cell line.

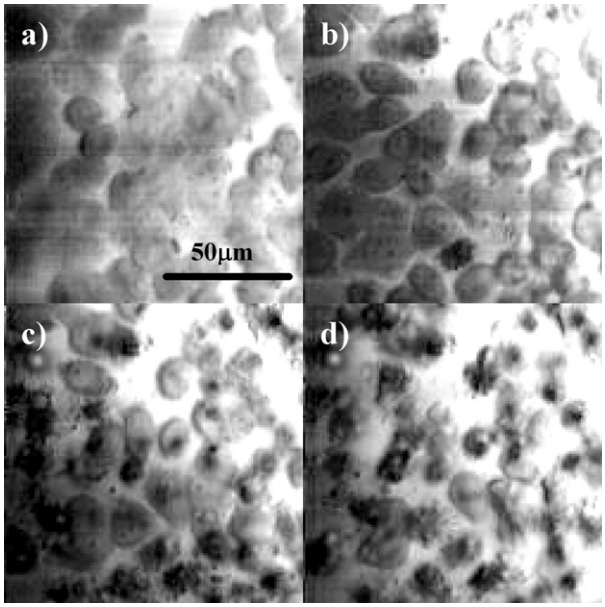

Fig. 6. Acoustic microscopy images of HeLa cells undergoing cell death during exposure to cisplatin for (a) 2.5 h, (b) 12 h, (c) 18 h and (d) 24 h.

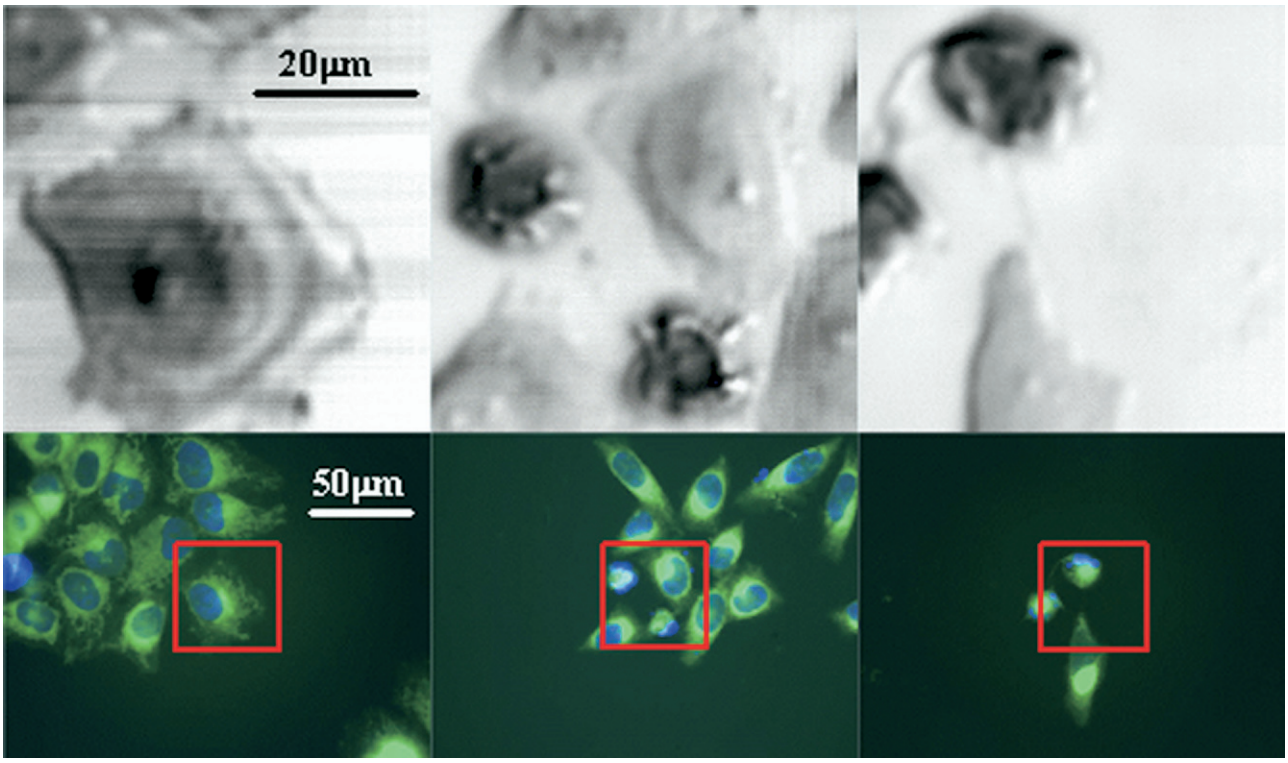

Fig. 7. Acoustic microscopy (top) and laser fluorescence (bottom) images of HeLa cells undergoing cell death during exposure to cisplatin for 0 h (left), 12 h (middle) and 24 h (right). Membranes were labeled with DIOC 5(3) (green) and condensed chromatin was labeled with H33342 (blue).

For HeLa cells, the slope of the normalized power spectrum increased from 0.35 dB/MHz to 0.52 dB/MHz after 24 h of treatment for signals obtained with the 20 MHz transducer. Increasing values were observed also for the 40 MHz transducer; however, this trend could not be confirmed as significant by ANOVA between the 0-h and the 24-h time point. The experimental set-up was the same for all scans throughout the experiments as were the ROI positions relative to the focus. Therefore, spectral slope values, as plotted in Fig. 3a, display relative changes caused by the treatment effect. Due to the smaller focal region, spectral slope values that are estimated in a ROI that might not be centered at the focus will be influenced by a constant offset only, without changing general the trend. The spectral slope was observed increasing as a function of treatment time.

In the model proposed by Lizzi et al. 1997a, assuming a random distribution of weak scatterers, increasing values for spectral slope correspond to a decrease in the effective scatterer size. During apoptosis, the nuclei condense (see Figs. 6 and 7) and, thus, the intact nucleus is replaced by multiple smaller condesed nuclei (apoptotic bodies) while undergoing apoptosis. This seems to be consistent with the experimental data in this study. For data obtained using the 20 MHz transducer, the spectral slope increases by 0.17 dB/MHz between 0 and 24 h of treatment while for the 40 MHz transducer, we have observed an increase of 0.035 dB/MHz. The application of ANOVA provided a p value of 0.167 for time dependent increasing spectral slope values of the 40 MHz data.

Figure 3b shows the backscatter coefficients at 0, 18 and 24 h after cisplatin exposure as a function of frequency. This parameter is commonly used in ultrasonic tissue characterization and describes the spectral dependence of the backscatter intensity. For HeLa cells, backscatter coefficients increased as a function of treatment time and allowed a differentiation between the three time points throughout the whole spectrum.

Acoustic attenuation of HeLa cells was estimated as a function of treatment time. The spectral substitution technique (Kuc 1985) was used and the reflector was placed at the transducers' focus to minimize variations. In these experiments, the sound reflection after propagating through the cell pellets and the reference reflection were recorded simultaneously using the two-chamber holder. This experimental set-up minimizes variations due to parameters that are hard to control because the same reflector surface is used for simultaneously recording the tissue measurement and the reference. As the attenuation estimation is based on the measurements of the reflection

from a strong reflector, they show smaller variation compared with backscatter measurements.

Figure 5a shows attenuation spectra in dB/cm at 0 h, 18 h and 24 h post-treatment. The resulting spectra, plotted for each time point in Fig. 5a, contain the attenuation spectra of the two different transducers, covering a range of 10-52 MHz and display that attenuation values increase as a function of treatment time. Small variations between the three different time points are recorded by the 20 MHz transducer and larger ones with the 40 MHz transducer. Attenuation spectra for the 18-h time point are approximately 5 dB/cm higher than for the 0-h time point. An increase of 5 dB/cm can also be observed between the 18-h and 24-h time point. The slopes of the attenuation spectra are plotted in dB/(MHz cm) as a function of treatment time in Fig.5b. For both transducers the acoustic attenuation increases by approximately 0.1 dB/(MHz cm) throughout the entire treatment time.

Acoustic microscopy

For the first time acoustic properties of single cells were imaged as a function of chemotherapeutic treatment using very high frequency ultrasound (0.9 GHz). Simultaneous optical microscopy and staining of cell compartments enabled the visualization of cellular structure optically and acoustically. An excellent correlation between the locations of increased attenuation in the acoustic images and the locations of apoptotic nuclear condensation, as determined by fluorescence staining, was observed. The contrast of the cell interior in the acoustic microscopy images increased for cells undergoing apoptosis. Cell shrinkage and nuclear condensation was observed in both acoustical and laser fluorescence images. The SASAM also allowed the monitoring of intracellular changes of acoustic properties throughout an entire treatment time course without staining, as the change in acoustic properties produced the contrast.

In acoustic microscopy, the signal intensity of a reflected pulse is measured for each image pixel. Since the intensity of each pulse represents acoustic attenuation along its path of sound propagation, the images can be directly related to the cells acoustic attenuation in the imaged spot. The apparent attenuation increase measured by the acoustic microscopy can be attributed to an increase in the cells' absorption or backscatter. Another possible influence on the received signal is the reflectivity of the boundary between the glass substrate and the cell. A change in density of the cell interior would change the reflectivity of that boundary and therefore influence the intensity of the detected pulse. Another reason for a variation of the signal intensity could be due to a change in the speed of sound that would cause defocusing. However, very large changes in speed of sound are required to produce these changes and, likely, cannot explain the observed effect. Acoustic microscopy images at this time provided a qualitative assessment of changes in acoustical properties of cells undergoing apoptosis. Since the images are currently qualitative, it cannot be stated with certainty what the observed changes represent. However, condensation and fragmentation of the nucleus will most likely result in higher scattering and thus in higher attenuation.

Using high frequency ultrasonic spectroscopy, it was shown that acoustic attenuation of HeLa cells increased as a function of treatment time as did the integrated backscatter coefficients. Because scattering reduces the energy of a transmitted pulse and, thus, increases attenuation, the increase in backscatter and attenuation obtained from spectroscopy and the increasing contrast of intra-cellular structures in acoustic microscopy images are potentially related. Due to the high acoustic attenuation in the 0.9 GHz frequency range, backscatter from the cell interior could not be detected with a sufficient signal-to-noise ratio. However, the changes in acoustic properties of the nucleus and nuclear fragments can help explain the increase in backscatter intensity observed in the high frequency ultrasound B-mode images. The nuclear condensation also potentially provides changes in scatterer size, spacing and distribution that might cause increasing backscatter intensity.

The subject of future work will be the clarification of unanswered questions arising from this work. The improvement of the signal-to-noise-ratio in acoustic microscopy will enable the detection of ultrasound backscatter of the cell interior and thus provide further information about the intracellular structure and acoustic properties. B-mode images of single cells that are obtained at the 0.9 GHz frequency range will also potentially allow ultrasound spectroscopy. Experiments performed in the frequency range from 10 MHz to 60 MHz can be improved by the use of thicker cell pellets. Due to apoptotic cell death, the amount of cells and, therefore, the thickness of the cell pellets decreased as a function of treatment time in the experiments described here. Further physical properties like density and acoustic impedance will be estimated using a newly designed holder for the cell pellets during the experiment. Apart from experimental studies investigating ultrasound backscatter from cells and tissues, theoretical modeling and the simulation of the scattering process will be a topic of future work to explore the influence of scatterer spacing and distribution in addition to the scatterer size, as it had been shown that scatterer spacing may also modify not only the backscatter intensity but also the spectral slope. As this work suggests that ultrasonic contrast during apoptosis is generated by structural changes in the cell and no staining is required, there is considerable potential to use this modality for the noninvasive detection of cell death.

Acknowledgments—The authors acknowledge the financial support of the Whitaker Foundation (grants RG-01-0141 and transitional funds),

the Natural Sciences and Engineering Research Council (NSERC, CHRP grant 237962–2000) and the Ontario Premier's Research Excellence Awards (PREA 00/5–0730). The VisualSonics ultrasound bio microscope was purchased with the financial support of the Canada Foundation for Innovation, the Ontario Innovation Trust and Ryerson University. The authors also thank Arthur Worthington, Gregory J. Czarnota and Anoja Giles for contribution to this work.

REFERENCES

Ackermann WW, Rabson A, Kurtz H. Growth characteristics of poliomyelitis virus in HeLa cell cultures – Lack of parallelism in cellular injury and virus increase. J Exp Med 1954;100:437–450.

Bereiter-Hahn J, Karl I, Luers H, Voth M. Mechanical basis of cell shape: Investigations with the scanning acoustic microscope. Biochem Cell Biol 1995;73:337–348.

Bereiter-Hahn J, Luers H. Subcellular tension fields and mechanical resistance of the lamella front related to the direction of locomotion. Cell Biochem Biophys 1998;29:243–262.

Brand S, Moerlein D, Rosner F, Wicke M, Jenderka KV. Estimation of intramuscular fat content (IMF) in the musculus longissimus dorsi (LD) of pigs by analysis of RF echo signals obtained from a clinical B-mode device. Proceedings of the 2002 IEEE Ultrasonics Symposium. IEEE, 2002:1333-1336.

Brand S, Czarnota GJ, Solanki B, Foster D, Kolios MC. Ultrasonic assessment of death in HEp2 cells using spectral and wavelet based analysis of backscattered RF-signals. Proceedings of the 2006 Ultrasonics Symposium. IEEE, 2006:626-629.

Briggs A. Acoustic microscopy, in monographs on the physics and chemistry of materials. Oxford: Clarendon Press, 1992.

Briggs A. Advances in acoustic microscopy. New York and London: Plenum Press, 1995.

Briggs G, Wang J, Gundle R. Quantitative acoustic microscopy of individual living human cells. J Microsc 1993;172:3–12.

Cloutier G, Qin Z. Ultrasound backscattering from nonaggregating and aggregating erythrocytes–A review. Biorheology 1997;34: 443–470.

Czarnota GJ, Kolios MC, Vaziri H, Benchimol S, Ottensmeyer FP, Sherar MD, Hunt JW. Ultrasonic imaging of viable, dead and apoptotic cells. Ultrasound Med Biol 1997;23:961–965.

Czarnota GJ, Kolios MC, Abraham J, Portnoy M, Ottensmeyer FP, Hunt JW, Sherar MD. Ultrasound imaging of apoptosis: High-resolution noninvasive monitoring of programmed cell death *in vitro*, *in situ* and *in vivo*. Br J Cancer 1999;81:520–527.

Dent CL, Scott MJ, Wickline SA, Hall CS. High-frequency ultrasound for quantitative characterization of myocardial edema. Ultrasound Med Biol 2000;26:375–384.

Duck FA. Physical properties of tissue. London: Academic Press, 1990.

Feleppa EJ, Lizzi FL, Coleman DJ, Yaremko MM. Diagnostic spectrum analysis in ophthalmology: A physical perspective. Ultrasound Med Biol 1986;12:623–631.

Feleppa EJ, Fair WR, Tsai H, Porter C, Balaji KC, Liu T, Kalisz A, Lizzi FL, Rosado A, Manolakis D, Gnadt W, Reuter VV, Miltner MJ. Progress in two-dimensional and three-dimensional ultrasonic tissue-type imaging of the prostate based on spectrum analysis and nonlinear classifiers. Mol Urol 1999;3:303–310.

Feleppa EJ, Fair WR, Liu T, Kalisz A, Balaji KC, Porter CR, Tsai H, Reuter V, Gnadt W, Miltner MJ. Three-dimensional ultrasound analyses of the prostate. Mol Urol 2000;4:133–139.

Feleppa EJ, Kalisz A, SokilMelgar JB, Lizzi FL, Liu T, Rosado AL, Shao MC, Fair WR, Wang Y, Cookson MS, Reuter VE, Heston WDW. Typing of prostate tissue by ultrasonic spectrum analysis. IEEE Trans Ultrason Ferroelectr Freq Contr 1996;43:609–619.

Feleppa EJ, Lizzi EL, Coleman DJ, Yaremko MM. Diagnostic spectrum analysis in ophthalmology: A physical perspective. Ultrasound Med Biol 1986;12:623–631.

Foster FS, Pavlin CJ, Harasiewicz KA, Christopher DA, Turnbull DH. Advances in ultrasound biomicroscopy. Ultrasound Med Biol 2000;26:1–27.

Gärtner T, Jenderka KV, Schneider H, Heynemann H. Tissue characterization by imaging of acoustical parameters. Acoust Imaging 1996;22:365–370.

Hunt JW, Worthington AE, Xuan A, Kolios MC, Czarnota GJ, Sherar M D. A model based upon pseudo regular spacing of cells combined with the randomisation of the nuclei can explain the significant changes in high-frequency ultrasound signals during apoptosis. Ultrasound Med Biol 2002;28:217–226.

Insana MF, Wagner RF, Brown DG, Hall TJ. Describing small-scale structure in random media using pulse-echo ultrasound. J Acoust Soc Am 1990;87:179–192.

Jenderka KV, Gärtner T, Zacharias M, Heynemann H, Cobet U. System independent tissue typing of human testis and prostate. Proc IEEE Ultrason Symp 1999;2:1377–1380.

Kolios MC, Czarnota GJ, Lee M, Hunt JW, Sherar MD. Ultrasonic spectral parameter characterization of apoptosis. Ultrasound Med Biol 2002;28:589–597.

Kolios MC, Taggart L, Baddour RE, Foster SF, Hunt JW, Czarnota GJ, Sherar MD. An investigation of backscatter power spectra from cells, cell pellets and microspheres. Proceedings of the 2003 IEEE International Ultrasonics Symposium. IEEE, 2003:606-609.

Kuc R. Estimating reflected ultrasound spectra from quantized signals. IEEE Trans Biomed Eng 1985;32:105–112.

Kundu T. Ultrasonic nondestructive evaluation: Engineering and biological material characterization. Boca Raton: CRC-Press LLC, 2004.

Kundu T, Bereiter-Hahn J, Hillmann K. Calculating acoustical properties of cells: Influence of surface topography and liquid layer between cell and substrate. J Acoust Soc Am 1992;91:3008–3017.

Kundu T, Bereiter-Hahn J, Karl I. Cell property determination from the acoustic microscope generated voltage versus frequency curves. Biophys J 2000;78:2270–2279.

Lahorte CM, Vanderheyden JL, Steinmetz N, Van de Wiele C, Dierckx RA, Slegers G. Apoptosis-detecting radioligands: Current state of the art and future perspectives. Eur J Nucl Med Mol Imaging 2004;31:887–919.

Lang M, Ermert H, Heuser L. *In vivo* study of online liver tissue classification based on envelope power spectrum analysis. Ultrason Imaging 1994;16:77–86.

Lemor M, Weiss EC, Pilarczyk G, Zinin PV. Measurements of elastic properties of cells using high-frequency time-resolved acoustic microscopy. Proceedings of the 2003 IEEE Ultrasonics Symposium. IEEE, 2003:881-884.

Lemor RM, Weiss EC, Pilarczyk G, Zinin PV. Mechanical properties of single cells - measurement possibilities using time-resolved scanning acoustic microscopy. Proceedings of the 2004 IEEE Ultrasonics Symposium. IEEE, 2004:622-629.

Lizzi FL, Greenebaum M, Feleppa EJ, Elbaum M, Coleman DJ. Theoretical framework for spectrum analysis in ultrasonic tissue characterization. J Acoust Soc Am 1983;73:1366–1373.

Lizzi FL, Ostromogilsky M, Feleppa EJ, Rorke MC, Yaremko MM. Relationship of ultrasonic spectral parameters to features of tissue microstructure. IEEE Trans Ultrason Ferroelectr Freq Control 1986;33:319–329.

Lizzi FL, King DL, et al. Comparison of theoretical scattering results and ultrasonic data from clinical liver examinations. Ultrasound Med Biol 1988;14:377–385.

Lizzi FL, Astor M, Feleppa EJ, Shao M, Kalisz A. Statistical framework for ultrasonic spectral parameter imaging. Ultrasound Med Biol 1997a;23:1371–1382.

Lizzi FL, Feleppa EJ, Astor M, Kalisz A. Statistics of ultrasonic spectral parameters for prostate and liver examinations. IEEE Trans Ultrason Ferroelectr Freq Control 1997b;44:935–942.

Lu ZF, Zagzebski JA, Lee FA. Ultrasound backscatter and attenuation in human liver with diffuse disease. Ultrasound Med Biol 1999;25: 1047–1054.

Madsen EL, Dong F, Frank GR, Garra BS, Wear KA, Wilson T, Zagzebski JA, Miller HL, Shung KK, Wang SH, Feleppa EJ, Liu T, O'Brien WD Jr, Topp KA, Sanghvi NT, Zaitsev AV, Hall TJ, Fowlkes JB, Kripfgans OD, Miller JG. Interlaboratory comparison of ultrasonic backscatter, attenuation, and speed measurements. J Ultrasound Med 1999; 18:615–631.

Maldonado V, Melendez J, Gonzalez H, Ortega A. Internucleosomal DNA cleavage in HeLa cells exposed to cisplatin. Biochem Mol Biol Int 1995;37:691–696.

Masters JR. HeLa cells 50 years on: The good, the bad and the ugly. Nat Rev Cancer 2002;2:315–319.
Moerlein D, Brand S, Rosner F, Wicke M, Jenderka KV. Nondestructive estimation of the intramuscular fat content of the longissimus muscle of pigs by means of spectral analysis of ultrasound echo signals. Meat Science 2005;69:187–199.
Nicholas, D. Time-frequency-domain analysis: One-dimensional phantom studies. Phys Med Biol 1982;27:665–682.
Oelze ML, O'Brien WD Jr. Improved scatterer property estimates from ultrasound backscatter for small gate lengths using a gate-edge correction factor. J Acoust Soc Am 2004;116:3212–3223.
Oosterveld BJ, Thijssen JM, Hartman PC, Romijn RL, Rosenbusch GJ. Ultrasound attenuation and texture analysis of diffuse liver disease: Methods and preliminary results. Phys Med Biol 1991;36:1039–1364.
Silverman RH, Rondeau MJ, Lizzi FL, Coleman DJ. Three-dimensional high-frequency ultrasonic parameter imaging of anterior segment pathology. Ophthalmology 1995;102: 837–843.
Silverman RH, Lizzi FL. High-resolution ultrasonic imaging and characterization of the ciliary body. Invest Ophthalmol Vis Sci 2001; 42:885–894.
Taggart L, Baddour RE, Giles A, Czarnota GJ, Kolios M. Ultrasonic characterization of whole cells and isolated nuclei. Ultrasound Med Biol 2007;33:389–401.
Thijssen JM. The history of ultrasound techniques in ophthalmology. Ultrasound Med Biol 1993;19:599–618.
Turnbull DH, Wilson SR, Hine AL, Foster FS. Ultrasonic characterization of selected renal tissues. Ultrasound Med Biol 1989;15:241–253.
Ursea R, Coleman DJ, Silverman RH, Lizzi FL, Daly SM, Harrison W. Correlation of high-frequency ultrasound backscatter with tumor microstructure in iris melanoma. Ophthalmology 1998;105:906–912.
Velazquez M, Maldonado V, Melendez-Zajgla J. Cisplatin-induced apoptosis of HeLa cells. Effect of RNA and protein synthesis inhibitors, Ca2+ chelators and zinc. J Exp Clin Cancer Res 1998; 17:277–284.
Verbeek AM, Thijssen JM, Cuypers MH, Brink H, Deutman AF. Echographic classification of intraocular tumours. A 15-year retrospective analysis. Acta Ophthalmol (Copenh) 1994;72:416–422.
Waters KR, Bridal SL, Cohen-Bacrie C, Levrier C, Forners P, Laugier P. Parametric analysis of carotid plaque using a clinical ultrasound imaging system. Ultrasound Med Biol 2003;29:1521–1530.
Weiss EC, Lemor RM, Pilarczyk G, Anastasiadis P, Zinin PV. Imaging of focal contacts of chicken heart muscle cells by high-frequency acoustic microscopy. Ultrasound Med Biol 2007;33:1320–1326.
Worthington AE, Sherar MD. Changes in ultrasound properties of porcine kidney tissue during heating. Ultrasound Med Biol 2001; 27:673–682.
Zuber M, Gerber K, Erne P. Myocardial tissue characterization in heart failure by real-time integrated backscatter. Eur J Ultrasound 1999; 9:135–143.
Zoller J, Brandle K, Bereiter-Hahn J. Cellular motility *in vitro* as revealed by scanning acoustic microscopy depends on cell-cell contacts. Cell Tissue Res 1997;290:43–50.

APPENDIX

SUPPLEMENTARY DATA

Supplementary data associated with this article can be found, in the online version, at doi:10.1016/j.ultrasmedbio.2007.11.001.

Video Clips cited in this article can be found online at: http://www.umbjournal.org.